Correlation models for next-generation amplitude and cumulative intensity measures using artificial neural networks

Savvinos Aristeidou M.EERI [ID], **Davit Shahnazaryan** [ID], and **Gerard J O'Reilly M.EERI** [ID]

Abstract

Various next-generation intensity measures (IMs) have emerged in recent years. For instance, filtered incremental velocity, $FIV3$, was shown to be efficient in predicting the collapse of structures, or average spectral acceleration, Sa_{avg}, shown to be well-correlated with a wide range of response, from initiation of structural damage yielding to structural collapse. Different ground motion models (GMMs) are available to predict the probabilistic distribution of these IMs, given a set of seismological parameters. Nonetheless, a few key correlation models are still missing in the literature, which are elemental for a more holistic approach to ground motion record selection. These models are vital when performing seismic hazard analysis and ground motion record selection using state-of-the-art approaches like the conditional spectrum or generalized conditional intensity measure (GCIM) methods. This study uses a single machine-learning-based generalized ground motion model (GGMM) to estimate all the IMs. The model is based on the Next-Generation Attenuation (NGA)-West2 database and was utilized to quantify the correlations between the residuals. Correlations were calculated for intra- and inter-event residuals, but only those for total residuals are presented here, given their utility. Since the calculation of residuals comes from the same GMM and the same database of ground motions, this produces more consistent correlation coefficients between all IMs. To facilitate the usage of these correlation coefficients, predictive models of the empirical data were developed using machine-learning-based techniques, namely artificial neural networks (ANNs). It was found that $FIV3$ is strongly correlated with $Sa(\sim 1\ s)$ and itself across all periods and has a weak

Centre for Training and Research on Reduction of Seismic Risk (ROSE Centre), Scuola Universitaria Superiore IUSS Pavia, Pavia, Italy

Corresponding author:
Gerard J O'Reilly, Centre for Training and Research on Reduction of Seismic Risk (ROSE Centre), Scuola Universitaria Superiore IUSS Pavia, Palazzo del Broletto, Piazza della Vittoria 15, Pavia 27100, Italy.
Email: gerard.oreilly@iusspavia.it

negative correlation with duration at short periods and near-zero correlation for longer periods. Also, a stronger negative correlation between *Sa* and significant duration was found, compared with other prominent existing models. Direct correlation models between *Sa* and Sa_{avg} are also proposed.

Introduction

Earthquake-induced ground motion severity can be quantified via a plethora of proxies describing the amplitude, frequency content, and duration of ground shaking, termed intensity measures (IMs). Traditionally, the ground motion amplitude and frequency content are explicitly considered by examining acceleration-based response spectrum quantities. However, other types of IMs, like duration, average spectral acceleration, or filtered incremental velocity, *FIV*3, have received less attention due to their relative novelty, despite being efficient predictors of structural response (Bojórquez et al., 2012). These "secondary" features of ground motion shaking (i.e., duration, average spectral intensity, energy content, and velocity-based IMs) are generally assumed to be implicitly accounted for by limiting the causal parameters (e.g., magnitude and source-to-site) of the selected ground motion record set (e.g., ASCE, 2017; Bommer and Acevedo, 2004; Spillatura et al., 2021).

To perform a non-linear response history analysis (NRHA), a set of ground motion records must be selected, which usually depends on the definition of a target spectrum. The set of records that is as close as possible to a target spectrum and its anticipated dispersion are usually chosen as input records for the NRHA. Earlier proposals and a few current seismic provisions (e.g., ASCE 7–10 and Eurocode 8) recommended using a uniform hazard spectrum (UHS) for *Sa* as the target spectrum. More recently, improved approaches introduced the concept of the conditional mean spectra and conditional spectra (CMS, and CS, respectively) (Baker and Cornell, 2006a, 2006b; Abrahamson and Al Atik, 2010; Baker, 2011), which provides median spectral ordinates and logarithmic standard deviations conditioned to the intensity at a certain period of vibration having a certain probability of exceedance level. More holistic ground motion record selection methods like the generalized conditional intensity measure (GCIM) method that considered the conditional distribution of IMs beyond spectral acceleration made it possible to explicitly consider several IMs during the selection process (Bradley, 2010). These methods require not only an available ground motion model (GMM) of each IM but also knowledge of correlations between the residuals of all IMs (or spectral ordination of the same IM) that are under consideration.

The GMM provides the marginal, or unconditional, distribution of an IM given specific causal parameters (Baker et al., 2021). To obtain conditional distributions of an IM with other relevant IMs, the correlations between them are needed. Despite several recent studies illustrating their appreciable predictive power and efficiency in seismic risk assessments, to the authors' knowledge, there are no correlation models of *FIV*3 with itself or with other IMs, nor is there a direct correlation model for Sa_{avg} with other IMs. Therefore, this study

attempts to close this gap while also refining a few conventional correlation models using machine learning-based techniques. In addition, these correlation models can find use in specialized performance-based hazard and risk assessments, where it is often required to estimate the joint probability of occurrence of different IMs through a vector-based probabilistic seismic hazard analysis (PSHA) (Bazzurro and Cornell, 2002). Further details on the general procedure of said vector-PSHA are formalized for the case of two IMs in (Baker et al., 2021) for interested readers.

First, the IMs and their cross-correlations are described in more detail. Then, a brief description of the estimation of residuals is given, along with the adopted GMM and strong-motion database. Subsequently, the methodology for computing the correlation coefficients is outlined, and the architecture of artificial neural network (ANN) models is presented. Finally, the quantified empirical correlations are appraised, and their comparisons with the fitted ANN models and other existing models are discussed.

A novelty of this article is the exploration of machine learning-based techniques, namely ANN, for the regression models of correlations. This is in contrast with the traditional approach of identifying functional forms, which in some cases might even deviate from empirical values in their estimations, thus introducing fitting errors. To the authors' knowledge, no such ANN models currently exist in the literature. This is the case for cross-IM correlations at a single site, although an advanced approach has been applied to the spatial correlation of IMs in a recent study (Bodenmann et al., 2023). Another (and most important) novelty of this study is bridging the gap in the correlations of *FIV*3 and direct estimation of Sa_{avg} with themselves and other conventional IMs. These IMs have been studied in many past works to demonstrate their utility in seismic response assessment, but often lack the necessary GMMs or correlation models to fully leverage them for ground motion selection, vector-PSHA, or generally account for these IMs in a site or regional assessment. In addition, the procedure adopted is modular in the sense that it could be easily extended to other IMs or horizontal component definitions through simple repository and model versioning and updating. These are the main novelties of this work, while at the same time, it was aimed to complement the existing body of literature regarding the more well-established IMs.

Correlation models developed

There are many different IMs that are of interest to seismic engineers, which generally depend on the type of structure under examination and the extent of the investigation. The IMs used for the correlations in this study, and the definitions of those IM are given in the following:

- **_PGA_**: peak ground acceleration.
- **_PGV_**: peak ground velocity.
- **_Sa(T)_**: 5%-damped spectral acceleration at a vibration period, *T*. List of periods: T = [0.01, 0.05, 0.1, 0.15, 0.2, 0.3, 0.4, 0.5, 0.6, 0.7, 0.8, 0.9, 1, 1.2, 1.4, 1.7, 2, 2.5, 3, 3.5, 4, 5] s.
- **_Ds_$_{\mathbf{xy}}$**: x%–y% significant duration, defined as the time interval over which x% to y% of the integral $\int_{0}^{t_{max}} [a(t)]^2 dt$ is accumulated (Trifunac and Brady, 1975), as per Equation 1. The proposed models include {x, y} = {5%,75%} and {x, y} = {5%, 95%}.

- ***Sa*_{avg}**: Sa_{avg}: average spectral acceleration as defined in Equation 3, for two different period ranges defined below. List of periods: $T =$ [0.1, 0.15, 0.2, 0.3, 0.4, 0.5, 0.7, 1, 1.5, 2, 2.5, 3, 3.5, 4] s.
- ***FIV*3**: $FIV3$: defined by Dávalos and Miranda (2019) and summarized in Equation 4. List of periods: $T =$ [0.1, 0.15, 0.2, 0.3, 0.4, 0.5, 0.7, 1, 1.5, 2, 2.5, 3, 3.5, 4] s.

PGA and *PGV* are included in the proposed models as they have traditionally been popular and are still used in simplified and/or regional seismic assessments (Akkar and Özen, 2005; Kaka and Atkinson, 2004; Borzi et al., 2015).

Regarding the importance of duration, Hancock and Bommer (2006) summarized how different conclusions have been drawn in the literature, depending on the structural demand parameters considered in each study. A few studies that considered only the peak structural deformations (Sarieddine and Lin, 2013) found that duration has little effect. Meanwhile, most other studies (Iervolino et al., 2006; Chandramohan et al., 2016; Oyarzo-Vera and Chouw, 2008; Raghunandan and Liel, 2013 Gentile and Galasso, 2021; Otárola et al., 2023) found that, while duration does not influence the peak deformations, it does influence the cumulative engineering demand parameters, and, therefore, the damage due to cumulative effects. Overall, it is generally important to consider the correlation of duration with *Sa* when examining the effects of duration on structural response, especially in degrading systems. Even though there are many ways to describe the duration of a strong ground motion (Bommer and Martínez-Pereira, 1999), the two most common definitions are bracketed duration and significant duration (Afshari and Stewart, 2016). The scope herein is limited to the significant duration since it is often the preferred definition used in the literature (e.g., Chandramohan et al., 2016). The significant duration is defined as follows:

$$Ds_{xy} = t_y - t_x \tag{1}$$

$$x = \frac{100\%}{I_a} \int_0^{t_x} [a(t)]^2 dt \tag{2}$$

where t_x and t_y are the time stamps on a Husid plot (Husid, 1969) at which $x\%$ and $y\%$ of the total Arias intensity, I_a, occurs (as defined in Equation 2 for x and similarly for y). The most common values of x and y adopted in the literature are $\{x, y\} = \{5\%, 75\%\}$ and $\{5\%, 95\%\}$, subsequently referred to as D_{S575} and D_{S595}, respectively.

Average spectral acceleration, Sa_{avg}, has been shown in the literature to be a better overall predictor of structural response, rather than the classic IM of *Sa* for the majority of structural typologies (e.g., Bianchini et al., 2009; Eads et al., 2015; Kazantzi and Vamvatsikos, 2015; O'Reilly, 2021a, 2021b). Different period ranges can be chosen for the definition of this IM depending on the structure and the level of inelasticity that one wants to capture more accurately. This ambiguity was investigated in several past works (Cordova et al., 2000; Vamvatsikos and Cornell, 2005), and also, an extensive analysis was conducted in Chapter 7 of Eads Miranda (2013), where it was explored how the range, number, and spacing of periods used to compute Sa_{avg} influences the efficiency of collapse risk assessment estimates of single-degree-of-freedom (SDOF), moment-resisting frames, shear wall, and reinforced concrete systems. Sa_{avg} was also included in the correlation models developed in this study. It is defined as the geometric mean of *N*-number spectral

accelerations at periods within a user-specified range [T_{lower}, T_{upper}], as expressed in Equation 3. Hence, 10 periods (i.e., $N = 10$) equally spanning each chosen period range were used (Eads et al., 2015). Two different period ranges were used for the proposed correlation models, [T_{lower}, T_{upper}] = [0.2 T, 2 T] and [0.2 T, 3 T], based on Kohrangi et al. (2017) and Eads et al. (2015) recommendations, respectively. The two Sa_{avg} metrics derived from different period ranges were treated as separate IMs, denoted as Sa_{avg2} and Sa_{avg3}, respectively. These different period ranges were adopted based on the different focus of the aforementioned articles. Eads et al. (2015) focused on the collapse prediction. In contrast, Kohrangi et al. (2017) were also interested in the floor-acceleration response and economic losses.

$$Sa_{avg} = \left[\prod_{i=1}^{N} Sa(c_i T) \right]^{1/N} \text{for} \begin{cases} c \in [0.2, 2] \text{ for } Sa_{avg2} \\ c \in [0.2, 3] \text{ for } Sa_{avg3} \end{cases} \tag{3}$$

Dávalos and Miranda (2019) proposed *FIV3* as a novel IM that showed promising results regarding its efficiency and sufficiency in characterizing the collapse performance of buildings. In addition, some recent studies further highlighted the value of this IM in estimating seismic collapse in buildings and bridges (Dávalos and Miranda, 2019, 2020; Aristeidou and O'Reilly, 2024). To date, there is just one empirical GMM for estimating this IM (Dávalos et al., 2020), whereas the other IMs tend to be better represented with several different GMM options. *FIV3* is briefly summarized mathematically as follows:

$$FIV3 = \max\{V_{s,max1} + V_{s,max2} + V_{s,max3}, |V_{s,min1} + V_{s,min2} + V_{s,min3}|\} \tag{4}$$

$$V_s(t) = \left\{ \int_{t}^{t+\propto \cdot T} \ddot{u}_{gf}(\tau)d\tau, \ \forall t < t_{end} - \propto \cdot T \right\} \tag{5}$$

where $V_s(t)$ is a series of incremental velocities, *IVs*, computed using time segments with duration $\alpha \cdot T$ via Equation 5, $V_{s,max1}$, $V_{s,max2}$, and $V_{s,max3}$ are the three local maxima *IVs* in $V_s(t)$ and $V_{s,min1}$, $V_{s,min2}$, and $V_{s,min3}$ are the three local minima *IVs* in $V_s(t)$, T, corresponds to the period of vibration of interest, t_{end} corresponds to the last instant of time of the acceleration time series, and $\ddot{u}_{gf}$ corresponds to the filtered acceleration time series using a second-order Butterworth low-pass filter with a cutoff frequency, f_c, equal to $\beta \cdot f$, where β is a scalar input that controls the f_c/f ratio. The α and β input parameters required to calculate Equation 4 were chosen as 0.7 and $1/f$ (or T), respectively, as these were the parameters chosen in the original study (Dávalos et al., 2020).

The *RotD50* horizontal component definition (Boore, 2010) was adopted for *PGA*, *PGV*, *Sa*, and *Sa*$_{avg}$, whereas the geometric mean of the two as-recorded horizontal components was adopted for *Ds* and *FIV3*, since other definitions have not been studied for these IMs so far. Baker and Bradley (2017) computed the spectral acceleration correlations for two horizontal component definitions (*RotD50* and *RotD100*) and concluded that they are essentially identical. This finding suggests that correlation models can be used interchangeably for the different common horizontal component definitions.

Table 1 summarizes the correlation models developed in this study, denoted as ASO24. Also summarized are a few pre-existing correlation models used for the comparisons herein. It should be noted that it is not an exhaustive list of pre-existing models, but rather a selection of models that used herein for comparative purposes. Listed in *italics* are a few

Table 1. Correlation models proposed here and corresponding existing ones from the literature. In *italics* are a few example models in the literature of pairs not examined herein, given for the sake of completeness.

IM_i \ IM_j	Sa	Sa_{avg2}	Sa_{avg3}	PGA	PGV	Ds_{575}	Ds_{595}	$FIV3$
Sa	ASO24, *BJ08, ASA14, BB17*	ASO24, *CB14 and BJ08*, *CB14 and ASA14**	ASO24, *CB14 and BJ08*, *CB14 and ASA14**	*BB17, TBB23*	*BB17, TBB23*	ASO24, *B11, BB17*	ASO24, *B11, BB17*	ASO24
Sa_{avg2}		ASO24	ASO24	ASO24	ASO24	ASO24	ASO24	ASO24
Sa_{avg3}			ASO24, *DM21*	ASO24	ASO24	ASO24	ASO24	ASO24
PGA					*BB17, TBB23*	*BB17, TBB23, B11*	*BB17, TBB23, B11*	ASO24
PGV						*BB17, TBB23, B11*	*BB17, TBB23, B11*	ASO24
Ds_{575}							*BB17, TBB23, B11*	ASO24
Ds_{595}								ASO24
$FIV3$								

ASO24: This study; BJ08: (Baker and Jayaram, 2008); ASA14: (Akkar et al., 2014); DM21: (Dávalos and Miranda, 2021); B11: (Bradley, 2011a); BB17: (Baker and Bradley, 2017); *: indirect method; TBB23: (Tarbali et al., 2023).

existing models (given as example) of the correlation pairs not examined herein. These pairs are not examined since first they do not find much use in contemporary seismic risk analysis applications, and second, they are already well documented in the literature (Baker and Bradley, 2017; Tarbali and Bradley, 2015; Tarbali et al., 2023). Cases noted as the "indirect method" for Sa_{avg} refer to the indirect method of estimating correlations, using the mathematical definition of Sa_{avg}, from Sa and exploiting the available models for that IM, which is described by Kohrangi et al. (2017).

Database and GMM

Regarding the GMM adopted in this study for the estimation of IM distributions, a single generalized ground motion model (GGMM) applicable to active shallow crustal tectonic regions was utilized. This model is presented by Aristeidou et al. (2024), and, therefore, not discussed in detail here. It was developed using the strong-motion database from NGA-West2 (Ancheta et al., 2013) using an ANN framework. Although other GMMs may have been used, only one was considered here to compute the residuals regarding these predictions. Studies such as Baker and Bradley (2017) have examined the impact of considering different GMMs and strong-motion databases when computing residuals and noted that while there is some difference, it is not considered to have a significant impact on the computed correlation coefficients. Therefore, it was deemed acceptable, and possibly advantageous, to use a single GGMM for all IMs examined herein. The ground motion database used is the same as the one used to develop the GGMM, namely the NGA-West2 database (Ancheta et al., 2013), and the same filtering criteria as described by Aristeidou et al. (2024) are applied and listed below:

- Only ground motion records from earthquakes with $M_w \geq 4.5$ were utilized. Earthquakes of lower magnitude were omitted as they were assumed not to be strong enough to induce significant non-linear deformations or structural collapse in engineered buildings without a significant amplitude scaling;
- Recordings with R_{rup} greater than 300 km were discarded;
- Recordings from instruments located on the free field, below the surface, or in the first story of low-rise structures (fewer than four stories) were utilized. This was based on the Geomatrix first letter code of the NGA-West2 flat file;
- Events with a hypocentral depth greater than 20 km were discarded;
- Events recorded on bedrock were discarded based on the upper threshold of 1300 m/s of mean shear wave velocities in the upper 30 m, $V_{s,30}$;
- Recordings from all event mechanisms (i.e., strike-slip, normal, reverse, reverse-oblique, and normal-oblique) from active shallow crustal tectonic environments were included;
- Only records whose minimum usable frequency of both components was less than 0.25 Hz were considered;
- Earthquakes with $M_w < 5.5$ and fewer than five recordings were discarded. Earthquakes with $5.5 \leq M_w < 6.5$ and fewer than three recordings were discarded. This was because those earthquakes could be considered to have insufficient number of recordings, and, therefore, unreliably recorded;
- Recordings were considered only if both horizontal components were available. This was necessary to characterize the different horizontal components of shaking;
- Recordings from aftershocks were excluded since most seismic hazard analyses are performed based on a (Poissonian) recurrence of mainshocks. Therefore, including
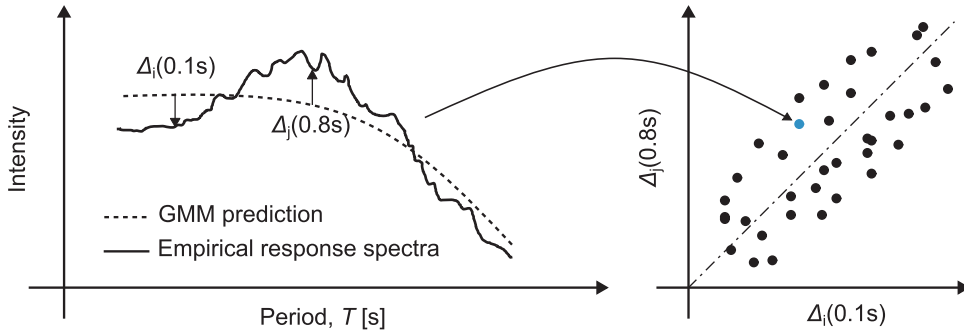
Figure 1. Schematic representation of the correlation between total residuals, Δ, (left) predicted and empirical response spectrum for a single record, and (right) residuals of the same IM from a large set of records.

aftershocks in the regression data set of the GGMM could introduce an unwanted bias. In this study, a recording is classified as an aftershock if it is defined as a "Class 2" event with centroid Joyner–Boore distance, $CR_{JB} < 10$ km according to the criteria given by Wooddell and Abrahamson (2014), although other classification criteria could have been used.

The basis of the filtering criteria was to remove some of the records that may be deemed unsuitable for general engineering use, which also indirectly form the recommended usage limitations of the correlation models. In total, they amounted to 4135 ground motion records from 102 earthquakes.

Methodology

To estimate the correlations between the aforementioned IMs, two important inputs are needed: a ground motion database and a GMM to predict the expected shaking intensity each rupture parameter. For each ground motion record in the database adopted, the residuals are computed as the difference between the actual observation (i.e., the ground motion record's actual value of IM) and the predicted median value from the GMM; as illustrated in Figure 1 for two values of a spectral IM. These residuals are computed for all IM definitions, the correlations between them are quantified, and predictive models were developed to estimate these correlations.

Inter-event, intra-event, and total residuals obtained from the GGMM were passed on to this study to compute the empirical cross-correlation of the IM residuals. Figure 2 depicts the empirical distributions of the normalized inter- and intra-event residuals for Ds_{595}, Sa ($T = 1$ s), and *FIV3* ($T = 1$ s). They are compared with the theoretical standard normal distribution and the Kolmogorov–Smirnov (KS) goodness-of-fit bounds at a 5% significance level. The compatibility of the GGMM with this data set is demonstrated by the observation that both inter- and intra-event empirical distributions lie within the KS goodness-of-fit bounds. Figure 2 depicts just three IMs but similar results were obtained for the other IMs considered, meaning that the natural logarithm of the residuals can generally be expected to be normally distributed, as is adopted in other past studies.
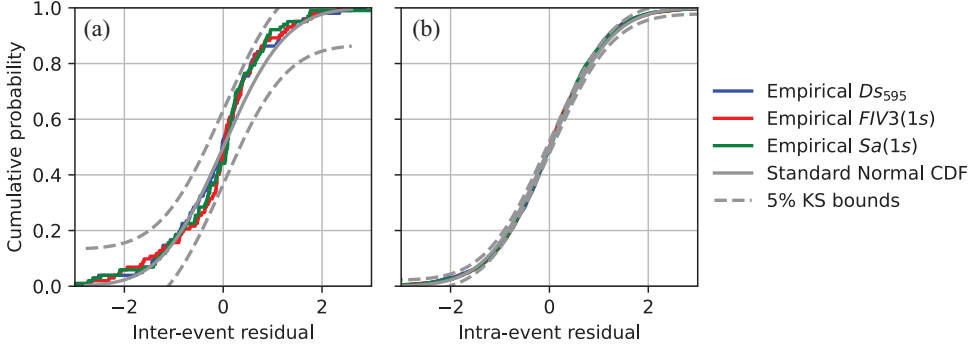
Figure 2. Empirical cumulative distribution of the (a) normalized inter-event and (b) normalized intra-event residuals obtained using the GGMM. Comparison with the theoretical standard normal cumulative distribution and the 5% KS bounds.

Even though Figure 1 focused on total (non-normalized) residuals, correlations are separately estimated for the normalized inter- and intra-event residuals, which are estimated from the mixed-effect regression of the GMM. Then, they are combined to derive the correlations of the normalized total residuals. The general methodology to achieve this is described below, beginning with the general form of the GGMM, given as:

$$\log_{10}IM_i = f_i(\boldsymbol{X}, \boldsymbol{\theta}) + \delta b_i \tau_i + \delta w_i \varphi_i \tag{6}$$

where $log_{10}(IM_i)$ is the logarithm with base 10 of the ith IM; $f_i(\boldsymbol{X}, \boldsymbol{\theta}) = \mu_{\log_{10}IM_i|X,\theta}$ is the predicted mean output from the ANN model, taking as input a set of causal parameters (M_{w}, R_{rup}, etc.), denoted as $\boldsymbol{X}$; $\boldsymbol{\theta}$ are the "calibrated coefficients" of the ANN model (i.e., synaptic weights and biases); δb_i and δw_i are the normalized inter- (between) and intra- (within) event residuals of IM_i, respectively; τ_i and φ_i are the inter- and intra-event logarithmic standard deviations. Here, lowercase δ is used to denote normalized residuals, and uppercase Δ is used to denote non-normalized residuals. The total normalized residual, δ_i, and total standard deviation, σ_i, can be expressed as the sum of inter- and intra-event residuals as:

$$\delta_i \sigma_i = \delta b_i \tau_i + \delta w_i \varphi_i \tag{7}$$

Combining Equations (6) and (7), and rearranging, the total normalized residual for a specific ground motion g, $\delta_{i, g}$, can be thought of as the number of standard deviations that the empirical IM is above the predicted mean value from the GMM, as illustrated in Figure 1 (albeit normalized with the total standard deviation) and formally described as:

$$\delta_{i, g} = \frac{\log_{10}IM_{i, g} - \mu_{\log_{10}IM_i|X,\boldsymbol{\theta}}}{\sigma_i} \tag{8}$$

It can be seen that $\log_{10}IM_{i, g}$ and $\delta_{i, g}$ exhibit a linear relationship in Equation 8; therefore by extension, the correlation between two IMs, for given causal parameters $\boldsymbol{X}$, is equal to the correlation between the normalized residuals, which in mathematical form translates to:

$$\rho_{\log_{10}IM_i|X,\boldsymbol{\theta},\ \log_{10}IM_j|X,\boldsymbol{\theta}} = \rho_{\delta_i, \delta_j} \tag{9}$$

Herein, for the sake of brevity, the correlation between two IMs will be simply referred to as ρ_{IM_i, IM_j}, where the conditioning on the causal parameters is implied but is generally taken as independent. Baker and Bradley (2017) studied the dependence of IM correlations on causal parameters such as magnitude, distance, and time-averaged shear wave velocity to 30 m depth, $V_{s,30}$. They found no systematic variation of these correlations with any of these GM causal parameters and corroborated this typical assumption that IM correlations are independent of these parameters (Baker and Cornell, 2005, Supplemental Appendix B; Huang and Galasso, 2019; Kohrangi et al., 2020; Tarbali et al., 2023), although other studies such as Kotha et al. (2017) have noted correlations to be magnitude-, region-, and database-dependent. It should be noted here that the correlations arising from *log10* transformations of IMs are eventually the same with the ones arising from natural logarithm transformations. In the literature, usually the natural logarithm transformation is used, thus the *ln* denotation can be used interchangeably.

Since δb_i and δw_i are generally assumed to be independent (Abrahamson et al., 2008), which was also the case in the recently developed GGMM used for this study, the correlations of inter- and intra-event residuals between different IMs can be estimated using the Pearson product-moment correlation coefficient formula (Ang and Tang, 1975), described as:

$$\rho_{x,y} = \frac{\sum_n [(x - \bar{x})(y - \bar{y})]}{\sqrt{\sum_n \left[(x - \bar{x})^2\right] \sum_n \left[(y - \bar{y})^2\right]}} \tag{10}$$

where x and y are generic variables, corresponding to δb_i and δb_j for inter-event correlation for IMs i and j, and to δw_i and δw_j for intra-event correlation in this application; $\bar{x}$ and $\bar{y}$ are the sample means, and Σ_n is the summation of all n ground motion records. Therefore, Equation 10 was used to compute the $\rho_{\delta bi,\delta bj}$ and $\rho_{\delta wi, \delta wj}$ correlations separately. From this definition of the correlation coefficient, the correlation between total residuals can be estimated from the individual inter- and intra-event correlations as follows:

$$\rho_{\delta_i, \delta_j} = \frac{\rho_{\delta b_i, \delta b_j} \tau_i \tau_j + \rho_{\delta w_i, \delta w_j} \varphi_i \varphi_j}{\sigma_i \sigma_j} \tag{11}$$

To account for the GMM uncertainty in the computed correlation coefficient, more than one GMM for active shallow crustal tectonic regions could be used with a logic tree; however, this was not applied here, and only a single GMM was used for simplicity. Past studies, such as Bradley (2011b), for example, have shown that the distribution of the correlation coefficient, which includes both finite sample size and GMM uncertainty, can be represented by the normal distribution. Herein, only point-estimate results for the mean correlation coefficients are presented. Finally, as previously mentioned, only the correlations between the total residuals are presented.

ANN architecture

The results of the empirical correlations calculated were then used to fit predictive models. Traditionally, these regression models (or predictive equations) are analytical functions with no strong physical basis and are developed simply to fit the observed data (e.g., Baker

and Chen, 2020; Baker and Cornell, 2006a; Baker and Jayaram, 2008). Because of this lack of physical basis, these analytical models may somewhat deviate from the empirical correlation data in some parts. To address this potential for sub-optimal fitting due to analytical functional form constraints, machine learning techniques were employed here. In particular, ANN (McCulloch and Pitts, 1943) was used to fit the data, eliminating the need to find suitable functional forms and keeping the misfit between observed and predicted data to a minimum. To the authors' knowledge, this technique has not been used to date for fitting predictive IM cross-correlation models.

To adopt this technique, an ANN architecture first needs to be set up and the optimal hyperparameters for each model need to be chosen. The general mathematical expression to predict the correlation between an IM_i-IM_j pair for the case of a neural network with one hidden layer is given as:

$$\rho_{\log_{10}IM_i,\ \log_{10}IM_j} = f_{activation2}\left[b_r + \sum_{h=1}^{n_h} W_{h,r} \cdot f_{activation1}\left(b_h + \sum_{p=1}^{n_p} W_{p,h} X_p\right)\right] \tag{12}$$

where X_p is the predictor feature p, $W_{p,h}$ is the weight of the connection between predictor neuron p and hidden neuron h, n_p is the number of predictor features, n_h is the number of hidden layer neurons, b_h is the bias of the hidden neuron h, $W_{h,r}$ is the weight of the connection between hidden neuron h and response neuron r, b_r is the bias of the response neuron r, $f_{activation1}$ and $f_{activation2}$ are the activation functions of the hidden and response layers, respectively. A natural logarithm transformation was applied to the predictor feature of only the following IM correlation pairs: Sa-Ds_{595}, Sa-Ds_{575}, Sa_{avg2}-Ds_{595}, Sa_{avg2}-Ds_{575}, Sa_{avg2}-PGA, Sa_{avg2}-PGV, Sa_{avg3}-Ds_{595}, Sa_{avg3}-Ds_{575}, Sa_{avg3}-PGA, and Sa_{avg3}-PGV.

A schematic representation of the network is illustrated in Figure 3 for the example case of the *Sa-FIV3* correlation model, where the weights, *W*, and biases, *b*, of the activation function are also depicted. It is noted here that the T_{IM} notation means period of the period-dependent IM, for example T_{Sa} means period of *Sa*. Meanwhile, the chosen hyperparameters for each model are listed in Table 2. Two hidden layers were required in most of the models to represent well the trends of the empirical data, with a high number of neurons per layer. Fewer neurons might also be adequate, but the goal was to resemble the empirical data as closely as possible, so having high number of neurons is more desirable, even though it creates relatively larger/heavier models. The activation functions are listed in Table 2 in the order of input, hidden, and output layers, respectively. *Softmax*, *linear*, *sigmoid*, and *tanh* activation functions were employed, as they were found to be optimal for the problem at hand. Despite the fact that the *softmax* activation function is primarily used for classification problems, it found usage here, as it was seen that for the regression problems at hand, in conjunction with other activation functions, to capture the empirical values very well. In addition, it was seen that the fit was very similar when either *softmax* or *sigmoid* was used. Also, a large number of epochs were chosen, as the goal here was to have the model predict values that are as close to the empirical ones as possible. In other words, overfitting here is desirable. Regarding the batch size, a small number were chosen in these models, since the training data set is exceptionally small (i.e., one correlation coefficient per unique IM pair). The hyperparameter selection for the predictive models was done manually for each model. This is because the regression problems at hands were relatively easy to tackle, so there was no need for automated hyperparameter selection methods (i.e., Bayesian optimization or grid search). The goal was to
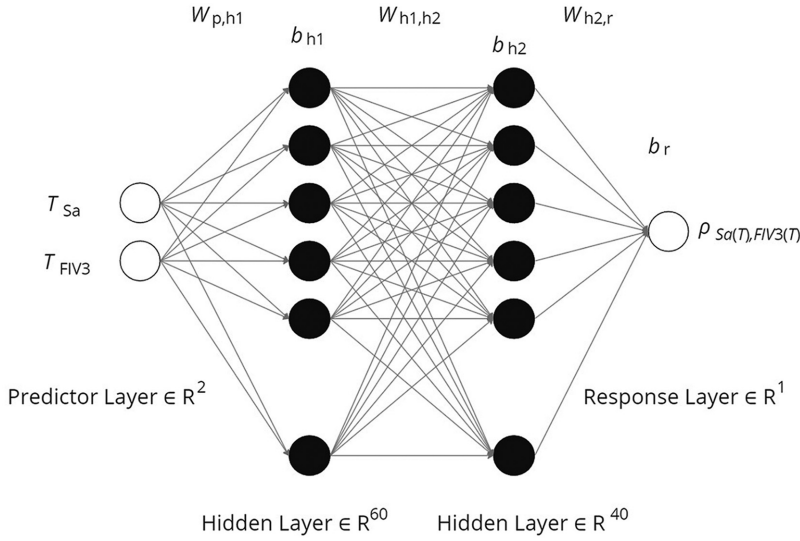
Figure 3. Schematic representation of ANN architecture for the case of *Sa-FIV3* correlation model.

reduce the mean squared error (MSE) metric as much as possible, while also observing visually the mismatch between empirical data and predictions. The first model fitted was the correlation between *Sa-FIV3*, for which the optimal hyperparameters, reported in Table 2, were found after a few attempts. For every subsequent correlation model, these parameters were tweaked accordingly to obtain a good fit for each case. It can be observed from the same table that each correlation model between different IM has different hyperparameters. This is because of different data size, different trends, and generally different values to fit. The MSE was selected as the loss function metric, which was minimized by the adaptive moment (ADAM) estimation algorithm (Kingma and Ba, 2014). Table 2 also reports two common indicators to assess the "goodness of fit" (i.e., MSE and coefficient of determination, R^2) for each correlation model. It can be seen that the all the MSE values are lower than 10^{-4}, and all the R^2 values higher than 0.98, which both indicate that the match between empirical values and predictions is good.

## Empirical results and model estimations

Correlations between traditional IMs

Of the 24 total IM cross-correlation models developed within this study, three are well-documented in the literature. Many past studies investigated and proposed parametric models and/or empirical tabulated values for the estimation of correlation between *Sa* of different periods (Akkar et al., 2014; Baker and Jayaram, 2008 Baker and Bradley, 2017), which is also examined here. The other well-documented models are *Sa-Ds$_{575}$* and *Sa-Ds$_{595}$*, for which the works of Bradley (2011a) and Baker and Bradley (2017) were used for the comparisons. The correlations estimated here are discussed further in this subsection and compared with the aforementioned existing models.

Correlation coefficients between $Sa(T_i)$ and $Sa(T_j)$ for four distinct values of T_j are illustrated in Figure 4, where any differences between the empirical and predicted values, or

Table 2. Key hyperparameters and general architecture of the adopted ANN correlation models.

Correlation model	Sa-$FIV3$	Sa-Sa	$FIV3$-$FIV3$	$FIV3$-Ds_{595}	$FIV3$-Ds_{575}	Sa-Ds_{595}	Sa-Ds_{575}	Sa-Sa_{avg3}	Sa-Sa_{avg2}	Sa_{avg2}-Sa_{avg2}	Sa_{avg3}-Sa_{avg3}	Sa_{avg3}-$FIV3$
Number of hidden layers	2	2	1	2	2	2	2	2	2	2	2	2
Activation functions	linear, sigmoid, tanh, linear	linear, sigmoid, sigmoid, linear	linear, softmax, linear	linear, softmax, linear, linear	linear, softmax, linear, linear	linear, sigmoid, softmax, linear	linear, sigmoid, softmax, linear	linear, tanh, sigmoid, linear	linear, tanh, sigmoid, linear	linear, sigmoid, sigmoid, linear	linear, sigmoid, sigmoid, linear	linear, sigmoid, sigmoid, linear
Number of neurons per hidden layer	60 and 40	60 and 30	300	30 and 30	30 and 30	40 and 60	40 and 60	60 and 40	60 and 40	60 and 30	60 and 30	60 and 30
Epochs	800	1000	3000	400	400	1500	1500	1000	1000	1300	1300	1000
batch size	8	8	16	4	4	4	4	8	8	8	8	8
MSE	3.04E-05	3.94E-05	4.32E-06	6.55E-06	5.38E-06	2.56E-05	2.66E-05	2.83E-05	4.12E-05	3.21E-05	4.64E-05	7.47E-05
R^2	0.9989	0.9991	0.9974	0.9990	0.9990	0.9994	0.9990	0.9990	0.9987	0.9988	0.9984	0.9971

| Correlation model	Sa_{avg3}-Ds_{595}	Sa_{avg3}-Ds_{575}	Sa_{avg2}-Sa_{avg3}	Sa_{avg3}-PGA	Sa_{avg3}-PGV	Sa_{avg2}-PGA	Sa_{avg2}-PGV	Sa_{avg2}-$FIV3$	Sa_{avg2}-Ds_{595}	Sa_{avg2}-Ds_{575}	$FIV3$-PGA	$FIV3$-PGV
Number of hidden layers	2	2	1	2	2	2	2	2	2	2	2	2
Activation functions	linear, softmax, softmax, linear	linear, softmax, softmax, linear	linear, softmax, linear	linear, softmax, softmax, linear	linear, softmax, softmax, linear	linear, softmax, softmax, linear	linear, softmax, softmax, linear	linear, sigmoid, sigmoid, linear	linear, softmax, softmax, linear	linear, softmax, softmax, linear	linear, softmax, tanh, linear	linear, softmax, tanh, linear
Number of neurons per hidden layer	60 and 40	60 and 40	300	60 and 40	60 and 40	60 and 40	60 and 40	60 and 30	60 and 40	60 and 40	40 and 40	50 and 50
Epochs	1500	1500	3000	1500	1500	1500	1500	1000	1500	1500	1600	1800
Batch size	4	4	16	4	4	4	4	8	4	4	4	4
MSE	4.60E-06	1.02E-05	2.00E-05	1.04E-06	5.82E-07	3.97E-06	4.81E-06	1.75E-05	9.89E-06	2.52E-05	9.44E-06	2.44E-06
R^2	0.9999	0.9996	0.9993	1.0000	0.9998	0.9999	0.9989	0.9993	0.9997	0.9990	0.9983	0.9940
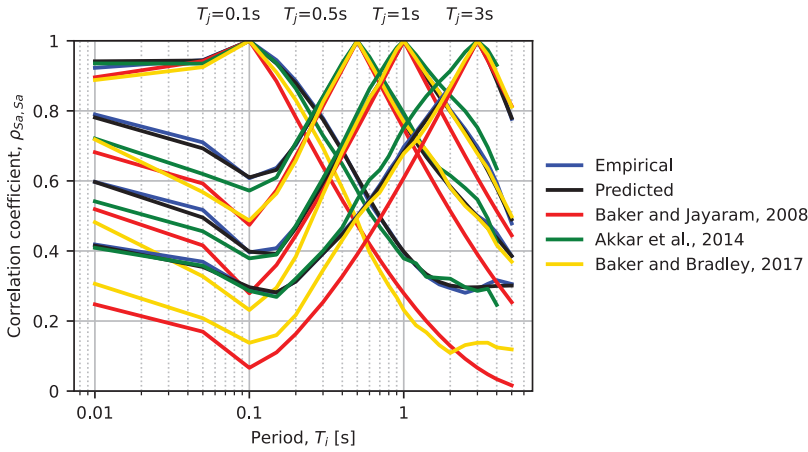
Figure 4. Correlation coefficients between $Sa(T_i)$ and $Sa(T_j)$ for four values of T_j.

differences between this and past studies, can be appreciated. First, it can be seen that the correlations predicted by the ANN model developed in this study are almost identical to the empirical data. This is seen throughout the range of values of the correlation model. This was very encouraging to see since it illustrates the utility of ANN models in this regard, which have yet to be employed for this purpose.

It can be observed that the correlations predicted by the Baker and Jayaram (2008) model somewhat deviate from the ones computed here, primarily where the inter-period "distance" increases. The BJ08 model generally underpredicts the correlations compared with the empirical data of this study. The impact of this underprediction on ground motion selection via conditional spectrum (Baker, 2011) would be that the variance around the target mean would be slightly higher, meaning that the selected ground motions would be more dispersed than they would be with using the proposed correlations. For structures where this spectral content at periods away from the conditioning period is relevant, it may result in an overprediction of structural demands. The difference of BJ08 model may be due to several factors. The most dominating factor was found to be the filtering of the ground motion records. Specifically, it was seen from background analyses (not presented here for brevity) that the limits on magnitude and distance ranges play the most important role. Other less important factors include first the difference in ground motion databases used, where BJ08 used the NGA-West database with approximately 2500 recordings available at moderate periods, whereas the proposed models utilized a subset of NGA-West2 database containing 4131 records. Second, small changes occur from the different GMM model from which the residuals are computed. Finally, the expected errors involved in functional form identification can also be anticipated to have a minor impact.

The model of Baker and Bradley (2017) is very close to BJ08, because of their very similar filtering criteria (i.e., the ones of Chiou and Youngs, 2008). However, BB17 presents higher correlations, in most period ranges, than BJ08, but still lower than the proposed values. Even though the same base database as the proposed model is used (i.e., NGA-West2), the filtering criteria are different, and that is the main cause of differences in the correlation values.
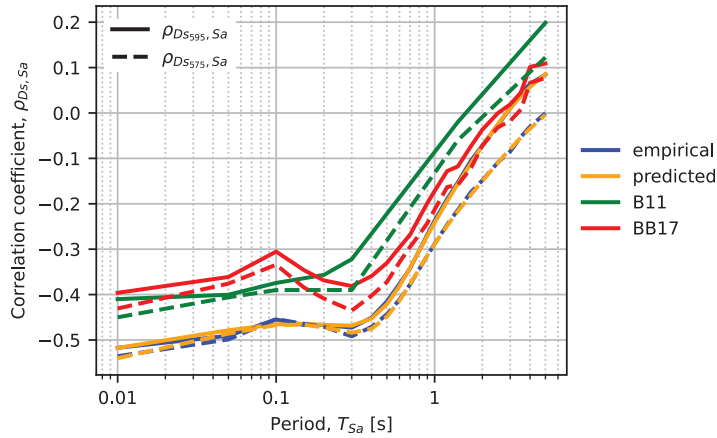
Figure 5. Empirical and predicted Sa-Ds_{595} and Sa-Ds_{575} correlation of the ANN and Bradley (2011a) models.

The model of Akkar et al. (2014) utilized strong-motion accelerograms from the RESORCE database (Akkar et al., 2014). It consists of 1041 accelerograms from 221 shallow active crustal earthquakes, most of which have epicentral locations in the Mediterranean region and the Middle East. The correlation coefficients for Sa up to 4 s are plotted, as this represents the maximum period input that the model can accommodate. The ASA14 correlations appear closely align with the ones calculated here and exhibit very similar trends. In addition, there is no sign of consistent underprediction or overprediction in any period ranges. Nevertheless, there is still a small deviation from the values of this study in specific parts. The main reason that the ASA14 model is closer to the proposed model is because they considered only events with magnitude larger than 4, from a data set which includes mostly events with magnitudes between 5 and 6. Meanwhile, the models of BJ08 and BB17 include much wider magnitude (>3) and distance (<400 km) filtering limits, from events and sites of assorted regions, resulting in higher aleatory variability, and, therefore, lower correlations. These are decisions that can potentially affect the eventual correlation coefficients.

In the case of significant duration, Figure 5 shows that the empirical correlation with Sa increases (i.e., takes less negative values) with increasing vibration period. The coefficients are monotonically increasing, except for the period range between 0.1–0.3 s, where the slope is transiently negative. This is caused by a sudden small increase in correlation for Sa(0.1 s), which is considered insignificant from a practical viewpoint. The same observations were also noticed by previous studies (Baker and Bradley, 2017; Bradley, 2011a), but can be a consequence of the available data rather than an underlying physical feature. Nevertheless, this behavior is regressed by a smooth, monotonically increasing, curve. Correlation of Sa with Ds_{575} is slightly more negative than the one with Ds_{595}, especially in longer periods of Sa. The fact that the correlation between Ds and high-period IMs (i.e., $Sa(T > 2$ s) and $FIV3(T > 1$ s) discussed later) is relatively small (i.e., weak linear relationship) suggests that ground motions with more energy concentrated in high periods do not translate to higher significant duration, or vice versa. Generally, duration exhibits a negative correlation with low-period IMs. This is an expected result since ground motions with longer-than-predicted durations tend to have their energy scattered over a longer
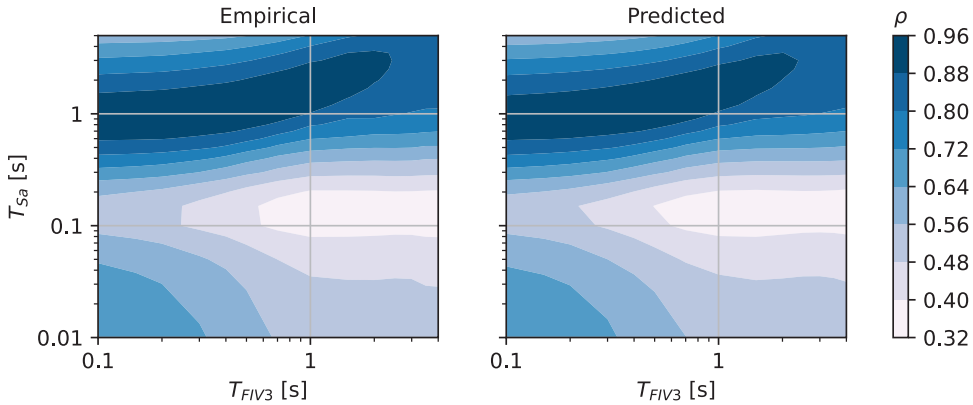
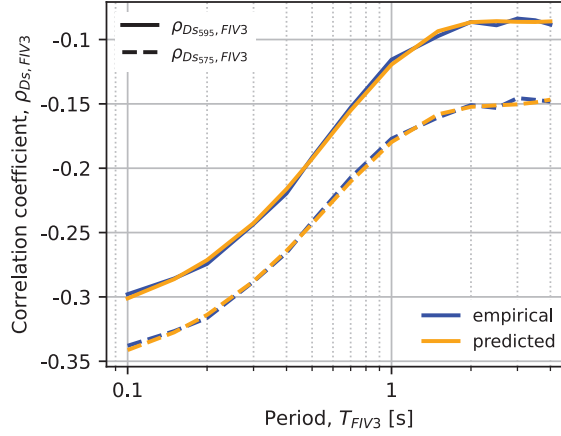**Figure 6.** Empirical and corresponding predicted correlation coefficients between *Sa* and *FIV3*.

period of time and are, therefore, less likely to cause large peak responses in a short-period damped oscillator. This is in contrast with long-period oscillators that resonate with longer duration of shaking and, therefore, present little or no negative correlation.

Regarding the comparison with the B11 model, the trend is very similar, but the correlations computed here are shifted downward by about 0.1 across the whole range of *Sa* periods. This is primarily due to the different filtering criteria and secondarily due to the difference in the ground motion database used (NGA-West1 versus NGA-West2), and the different GMMs employed. Also, the total number of ground motions utilized in that study was 1842. The BB17 correlations are more in line with the B11 correlations for low periods, and they converge to the proposed $\rho_{Ds_{595}, Sa}$ for long periods. As stated above, the difference is mostly due to the filtering of the ground motion database, since BB17 also used the NGA-West2 database.

Correlations between traditional and next-generation IMs

To select ground motions via the CS or GCIM methods that match the distribution of next-generation IMs conditioned on traditional IMs, which is often the goal of a more advanced ground motion record selection, the correlations between those traditional and next-generation IMs are needed. A few of those models are presented in this subsection. For instance, Figure 6 presents the observed/empirical and predicted correlations between *Sa* and *FIV3*. The empirical coefficient values range from 0.35 to 0.95. The results indicate that *FIV3* of most periods is highly correlated with *Sa*(1 s), which is the IM recommended by HAZUS (2003) to be used for seismic assessment of bridges in the United States. Also shown in Figure 6 are the corresponding predictions by the proposed ANN model, which capture the empirical data very well, as can be concluded by a visual inspection.

Figure 7 illustrates the empirical and predicted correlation coefficients of Ds_{595}-*FIV3* and Ds_{575}-*FIV3*. First, it can be observed that the correlation of Ds_{595}-*FIV3* is negative for all periods of *FIV3*, with values ranging from -0.3 for the lowest period *FIV3* to about -0.08 for the highest period *FIV3*. The trend is monotonically increasing and plateauing after an *FIV3* of period 2 s. The negative correlation coefficients suggest that a ground motion with a higher-than-predicted *FIV3* will, on average, have a lower-than-predicted duration. This was suspected to be attributed to the ground motion releasing all of its

Figure 7. Empirical and corresponding predicted correlation coefficients between Ds_{595}-*FIV*3 and Ds_{575}-*FIV*3.

energy within a few strong velocity pulses rather than over a long duration; however, the work of Tarbali et al. (2023) studied the effect of near-fault directivity pulses on correlations between Ds and other IMs and found that the effect was essentially negligible. Any differences found in that study were mainly attributed to the data set ground motion distribution and sample size, rather than the inherited characteristics of directivity pulse-like records. Overall, the trend of Ds-*FIV*3 correlations is very similar to the correlation trend between Sa and Ds, shown previously in Figure 5. For the case of Ds_{575}, the coefficients are shifted down by about 0.05. The empirical results suggest that *FIV*3 is more correlated with Sa than Ds_{595}.

Regarding the correlation between Sa and Sa_{avg3}, the difference or similarity between empirical and predicted coefficients can be assessed visually in Figure 8, where slices of two different periods of Sa_{avg3} are presented as demonstrative examples. From that, it can be concluded that the match between empirical and predicted values is excellent. As expected, the Sa_{avg3} of period T_i best correlates with Sa of period somewhat higher than T_i. Very similar results were found for the case of Sa_{avg2}, but not presented here due to space limitations. Kohrangi et al. (2017) presented an approach to develop a CS for Sa conditioned on a specific value of Sa_{avg} at the period of interest. This was done with the so-called "indirect" and "direct" methods, while comparing the two. The indirect method included in Figure 8 uses the CB14 GMM and BJ08 correlation model for the first case and the CB14 GMM and ASA14 correlation model for the second case. The main difference in the indirect methods here comes from the correlation models, rather than the GMM since it was generally found that the CB14 model predicts almost identical Sa values as the GMM used here (Aristeidou et al., 2024). Thus, the indirect method that uses the ASA14 correlation model results in about the same correlation coefficients as the proposed model, which is an encouraging result as it also provides a sort of validation to that theoretical development. That is because the ASA14 model itself is closer to the Sa-Sa correlation model proposed here than the BJ08 correlation model.

Figure 9 illustrates the empirical and predicted correlation coefficients of Sa_{avg3}-Ds_{595} and Sa_{avg3}-Ds_{575}. They are closely resembling the ones between Sa and Ds. The most negative correlation is found in the shortest period of Sa_{avg3}, while for long periods of Sa_{avg3},
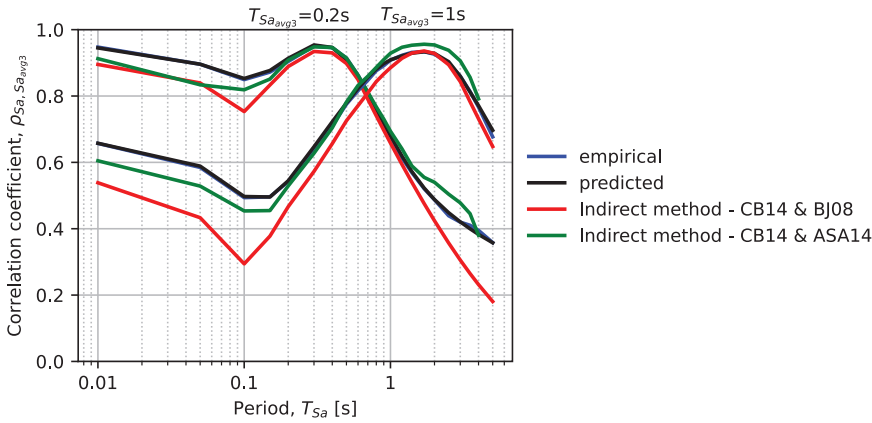
Figure 8. Correlation coefficients between $Sa(T_i)$ and $Sa_{avg3}(T_j)$ for two values of T_j.

the correlation with Ds takes smaller negative values and eventually approaches zero at a period of 4 s for the case of Ds_{595}. Meanwhile, the correlation with Ds_{575} is generally more negative, with the difference getting amplified in longer periods of Sa_{avg3}. The predicted coefficients almost overlap the empirical ones.

Correlations between next-generation IMs

Next-generation IMs showed improved performance in predicting different levels of non-linear behavior and collapse estimation in several past studies. Therefore, one may utilize one of the most recent record selection methodologies to consider the conditional distribution of a set of next-generation IMs when performing seismic risk studies.

Figure 10 shows the inter-IM correlations of $FIV3$ at different periods, with empirical correlation coefficients ranging from about 0.86 to 1, which suggests that $FIV3$ is strongly correlated between itself at different periods. This can be better appreciated in Figure 11, illustrating these same data slightly differently whereby specific slices of Figure 10 are shown. Also shown are the Sa-Sa correlations that were discussed in a previous subsection. This relative comparison affirms that $FIV3$ is much more correlated to itself across different periods than Sa. This signifies that $FIV3$ can be treated as almost a period-independent IM, in a similar way that PGA has been used traditionally, but with the added value of much-improved efficiency in its near-collapse response prediction, as past studies have noted. Also noted are the close predicted coefficients to the empirical ones, confirming the precision of the model. To the best of the authors' knowledge, there are no available correlation models of $FIV3$ with any other IM or with itself, which constitutes a novelty of this study.

The empirical and predicted correlation coefficients between Sa_{avg3} and $FIV3$ are presented in Figure 12, and they closely resemble the ones between Sa and $FIV3$. It can be noticed that the Sa_{avg3} at a period of about 1 s is well-correlated with $FIV3$ of most periods.

Figure 13 presents two slices of correlation coefficients between Sa_{avg3} for the case of periods 0.2 and 1 s. Also superimposed is the corresponding model proposed by Dávalos and Miranda (2021), which features the same period range for Sa_{avg} as the one used here
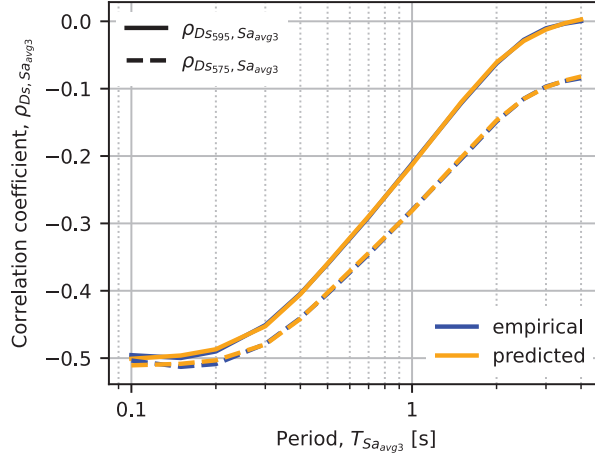
Figure 9. Empirical and corresponding predicted correlation coefficients of Sa_{avg3}-Ds_{595} and Sa_{avg3}-Ds_{575}.
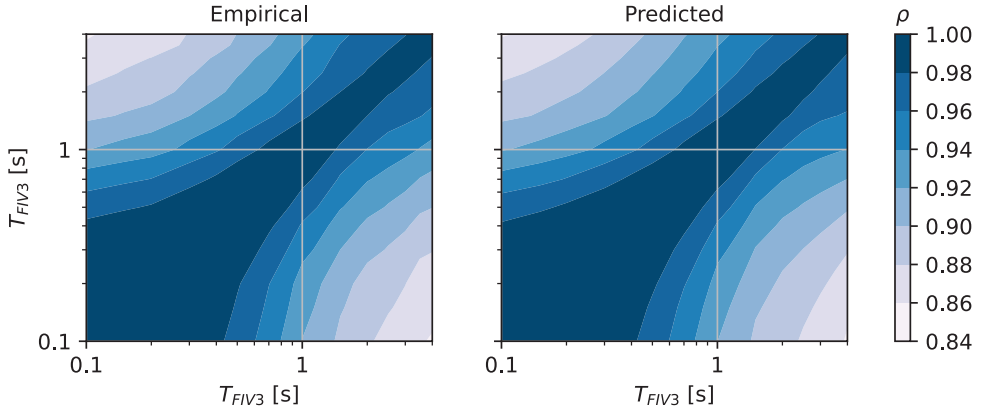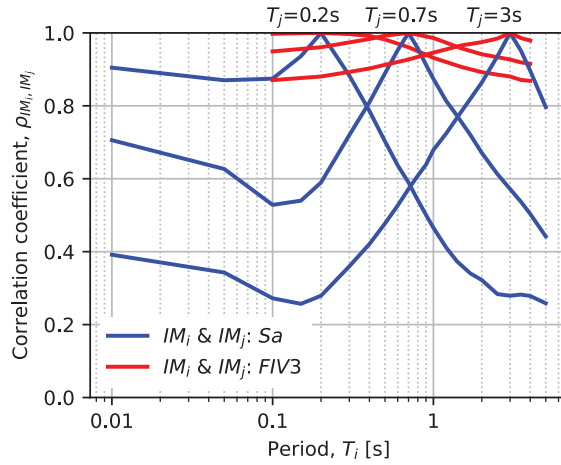

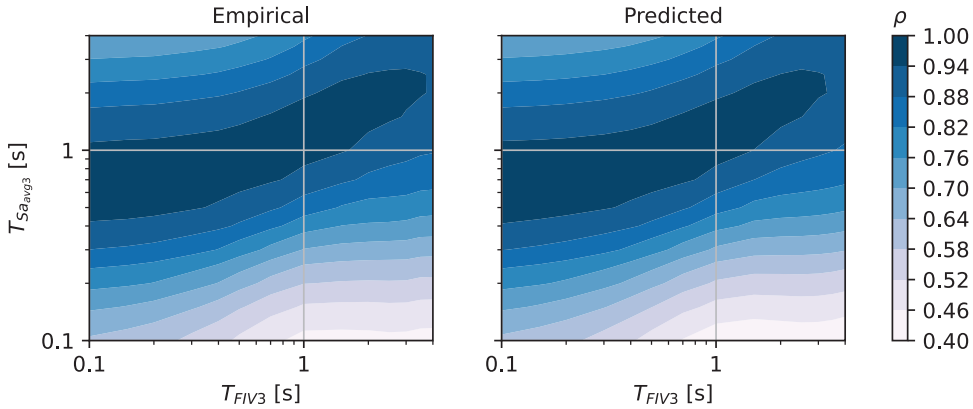**Figure 10.** Empirical and corresponding predicted correlation coefficients between $FIV3$ of different periods.

for Sa_{avg3}. The DM21 model underpredicts the correlation coefficients calculated here, which could be attributed to the different filtered data set used for the regression of the GMM and for the correlation model. For instance, one difference could be the filtering of the $V_{s,30}$ values, which were limited between 180 and 360 m/s, corresponding to National Earthquake Hazards Reduction Program (NEHRP) site class D. In any case, further investigations are needed to identify the precise cause of this difference. The display of contours of empirical and predicted correlation coefficients was omitted here for brevity.

Discussion and conclusion

This study presented the empirical correlations between assorted IMs of various types, namely PGA, PGV, spectral acceleration, Sa, significant duration, Ds, average spectral

Figure 11. Empirical correlation coefficients between $Sa(T_i)$-$Sa(T_j)$ and $FIV3(T_i)$-$FIV3(T_j)$ for three values of T_j.


Figure 12. Empirical and corresponding predicted correlation coefficients between Sa_{avg3} and $FIV3$.

acceleration, Sa_{avg}, and filtered incremental velocity, $FIV3$. The residuals, which are used for the calculation of correlations, were obtained from a previously developed GGMM and the same filtered ground motion database. This is believed to produce more consistent correlation coefficients since the same filtered database is used for the development of the GMM and the calculation of residuals used for the calculation of empirical correlation coefficients.

In total, 24 correlation predictive models were developed based on a novel approach via ANNs for the regression. It was shown how these models could excellently and adaptively fit the empirical data. Well-established correlation models from the literature were used to compare with the empirical and ANN-based correlation models proposed here. Based on the results, the following conclusions can be drawn from this research:

- Comparing correlations between traditional IMs with pre-existing models instills confidence in the empirical correlation coefficient computations and the sensibility
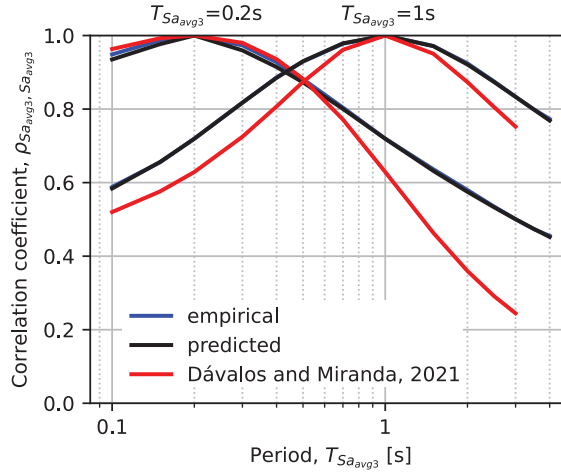
Figure 13. Correlation coefficients between $Sa_{avg3}(T_i)$ and $Sa_{avg3}(T_j)$ for two values of T_j.

of estimated residuals. That stems from the close alignment of their values to the empirical data, or at least their consistent adherence to the same trends.

- The *FIV*3 presented a relatively strong correlation with *Sa*, especially in the range of $Sa(T = 0.6\ \text{s})$ to $Sa(T = 3\ \text{s})$, which indicates that *FIV*3 is best correlated with moderate- and long-period IMs and less correlated with short-period IMs.
- The correlation between *Ds* and *FIV*3 showed the same trend as that of *Ds* and *Sa* but with a slightly weaker negative correlation (i.e., taking values closer to 0).
- The direct correlation between *Sa* and Sa_{avg}, developed here as a novel correlation model, will allow for more consistent ground motion record selection procedures when both of these IMs are considered, as several studies have already been carried out via an indirect method.
- The correlation between *Ds* and Sa_{avg3} closely resembles that of *Ds* and *Sa*.
- It was found that *FIV*3 is strongly correlated with itself, with the correlation values not dropping below 0.86, essentially making this IM almost period-independent, which could be useful for more general and regional studies.
- Correlation between *FIV*3 and Sa_{avg} exhibits similar behavior to that of *FIV*3 and *Sa*.
- The correlation models between Sa_{avg} spectral ordinates of different periods can be used to create a conditional spectrum based on Sa_{avg}, instead of *Sa*. The higher inter-IM correlations and lower dispersions of Sa_{avg} will produce spectra with less pronounced pinching at the conditional period and smaller spectral ordinates than CS based on *Sa*.
- The empirical results obtained in this study present some differences when compared to existing models, which were attributed mainly to the differences in the filtered database, and secondary to the utilized GMM and base database. It was seen that the fitting methodology of the existing models has negligible effect.
- The proposed predictive ANN models estimate the empirical data with high precision, as confirmed by the reported low MSEs, and high coefficients of determination. Simultaneously, it facilitates a seamless application since the models are readily available online.

Finally, a few correlation models have not been presented here graphically due to space limitations and information redundancy. Nevertheless, their coefficients can be obtained from the data provided online. The period range of applicability of these correlation models spans from 0.01 s to 5 s for Sa, 0.1 s to 4 s for Sa_{avg}, and 0.1 s to 4 s for $FIV3$. The ground motion causal parameters' range of applicability can be taken as the minimum and maximum value of each predictor feature used in the development of GGMM (Aristeidou et al., 2024). The same methodology and similar network architectures can be adapted to seamlessly come up with correlation models between other IMs or other horizontal component definitions. Overall, the models presented in this study represent a notable step toward allowing seismic risk analysts to adopt these next-generation IMs in their studies and account for their cross-correlations during ground motion record selection.

ORCID iDs

Savvinos Aristeidou (iD) https://orcid.org/0000-0002-4224-7891
Davit Shahnazaryan (iD) https://orcid.org/0000-0002-0529-5763
Gerard J. O'Reilly (iD) https://orcid.org/0000-0001-5497-030X

Data and resource availability

The relevant files and functions that can be used to get the correlation models' estimations presented here are available on GitHub at: https://github.com/Savvinos-Aristeidou/ANN_correlation_models.git. The user has the option of choosing whether they want to get the correlation values from the raw empirical tabulated values, via linear interpolation, or from the predictive model fitted with ANN. It is worth noting that there is no need to load any specific Python package to use the ANN models, but rather the code loads a file with all the fitted coefficients (i.e., weights and biases) and the activation functions and uses the ANN analytical functional form to output the correlation values.

References

Abrahamson N, Atkinson G, Boore D, Bozorgina Y, Campbell K, Chiou B, Silva W and Youngs R (2008) Comparisons of the NGA ground-motion relations. *Earthquake Spectra* 24(1): 45–66.
Abrahamson NA and Al Atik L (2010) Scenario spectra for design ground motions and risk calculation. In: *Proceedings of 9th US National and 10th Canadian conference on earthquake engineering, earthquake engineering research institute*, Oakland, CA, 25–29 July.

Afshari K and Stewart JP (2016) Physically parameterized prediction equations for significant duration in active crustal regions. *Earthquake Spectra* 32(4): 2057–2081.

Akkar S, Sandıkkaya MA, Şenyurt M, Azari Sisi A, Ay BÖ, Traversa P, Douglas J, Cotton F, Luzi L, Hernandez B and Godey S (2014) Reference database for seismic ground-motion in Europe (RESORCE). *Bulletin of Earthquake Engineering* 12(1): 311–339.

Akkar S and ÖzenÖ (2005) Effect of peak ground velocity on deformation demands for SDOF systems. *Earthquake Engineering & Structural Dynamics* 34(13): 1551–1571.

Akkar S, Sandıkkaya MA and Ay BÖ (2014) Compatible ground-motion prediction equations for damping scaling factors and vertical-to-horizontal spectral amplitude ratios for the broader Europe region. *Bulletin of Earthquake Engineering* 12(1): 517–547.

Ancheta TD, Darragh RB, Stewart JP, Seyhan E, Silva WJ, Chiou BSJ, Wooddell KE, Graves RW, Kottke AR, Boore DM, Kishida T and Donahue JL (2013) *PEER NGA-West2 Database*. Technical Report, PEER: 2013/03. Pacific Earthquake Engineering Research Center, University of California, Berkeley, CA.

Ang AH-S and Tang WH (1975) *Probability Concepts in Engineering Planning and Design: Decision, Risk and Reliability*. Hoboken, NJ: John Wiley & Sons. Available at: https://books.google.it/books?id=tuRDAQAAIAAJ

Aristeidou S and O'Reilly GJ (2024) Exploring the use of orientation-independent inelastic spectral displacements in the seismic assessment of bridges. *Journal of Earthquake Engineering*. Epub ahead of print 22 April. DOI: 10.1080/13632469.2024.2343067

Aristeidou S, Shahnazaryan D and O'Reilly GJ (2024) Artificial neural network-based ground motion model for next-generation seismic intensity measures. *Soil Dynamics and Earthquake Engineering* 184: 108851.

ASCE (2017) *Minimum Design Loads for Buildings and Other Structures* (ASCE 7-16). Reston, VI: American Society of Civil Engineers.

Baker J, Bradley B and Stafford P (2021) *Seismic Hazard and Risk Analysis*. 1st ed. Cambridge: Cambridge University Press.

Baker JW (2011) Conditional mean spectrum: Tool for ground-motion selection. *Journal of Structural Engineering* 137(3): 322–331.

Baker JW and Bradley BA (2017) Intensity measure correlations observed in the NGA-West2 database, and dependence of correlations on rupture and site parameters. *Earthquake Spectra* 33(1): 145–156.

Baker JW and Chen Y (2020) Ground motion spatial correlation fitting methods and estimation uncertainty. *Earthquake Engineering and Structural Dynamics* 49(15): 1662–1681.

Baker JW and Cornell CA (2005) *Vector-valued Ground Motion Intensity Measures for Probabilistic Seismic Demand Analysis*, John A. Blume Earthquake Engineering Center, Stanford University, Stanford, CA.

Baker JW and Cornell CA (2006a) Correlation of response spectral values for multicomponent ground motions. *Bulletin of the Seismological Society of America* 96(1): 215–227.

Baker JW and Cornell CA (2006b) Spectral shape, epsilon and record selection. *Earthquake Engineering & Structural Dynamics* 35(9): 1077–1095.

Baker JW and Jayaram N (2008) Correlation of spectral acceleration values from NGA ground motion models. *Earthquake Spectra* 24(1): 299–317.

Bazzurro P and Cornell CA (2002) Vector-valued probabilistic seismic hazard analysis (VPSHA). In: *Proceedings of the 7th US national conference on earthquake engineering*, Boston, MA, 21–25 July.

Bianchini M, Diotallevi PP and Baker JW (2009) Prediction of inelastic structural response using an average of spectral accelerations. In: *Proceedings of the 10th international conference on structural safety and reliability ICOSSAR09*, Osaka, Japan, 13–17 September.

Bodenmann L, Baker JW and Stojadinović B (2023) Accounting for path and site effects in spatial ground-motion correlation models using Bayesian inference. *Natural Hazards and Earth System Sciences* 23(7): 2387–2402.

Bojórquez E, Iervolino I, Reyes-Salazar A and Ruiz SE (2012) Comparing vector-valued intensity measures for fragility analysis of steel frames in the case of narrow-band ground motions. *Engineering Structures* 45: 472–480.

Bommer JJ and Acevedo AB (2004) The use of real accelerograms as input to dynamic analysis. *Journal of Earthquake Engineering* 8(1): 43–91.

Bommer JJ and Martínez-Pereira A (1999) The effective duration of earthquake strong motion. *Journal of Earthquake Engineering* 3(2): 127–172.

Boore DM (2010) Orientation-independent, nongeometric-mean measures of seismic intensity from two horizontal components of motion. *Bulletin of the Seismological Society of America* 100(4): 1830–1835.

Borzi B, Ceresa P, Franchin P, Noto F, Calvi GM and Pinto PE (2015) Seismic vulnerability of the Italian roadway bridge stock. *Earthquake Spectra* 31(4): 2137–2161.

Bradley BA (2010) A generalized conditional intensity measure approach and holistic ground-motion selection. *Earthquake Engineering and Structural Dynamics* 39(12): 1321–1342.

Bradley BA (2011a) Correlation of significant duration with amplitude and cumulative intensity measures and its use in ground motion selection. *Journal of Earthquake Engineering* 15(6): 809–832.

Bradley BA (2011b) Empirical equations for the prediction of displacement spectrum intensity and its correlation with other intensity measures. *Soil Dynamics and Earthquake Engineering* 31(8): 1182–1191.

Chandramohan R, Baker JW and Deierlein GG (2016) Quantifying the influence of ground motion duration on structural collapse capacity using spectrally equivalent records. *Earthquake Spectra* 32(2): 927–950.

Chiou BSJ and Youngs RR (2008) An NGA model for the average horizontal component of peak ground motion and response spectra. *Earthquake Spectra* 24(1): 173–215.

Cordova P, Deierlein G, Mehanny S and Cornell C (2000) Development of a two-parameter seismic intensity measure and probabilistic assessment procedure. In: *The Second US-Japan workshop on performance-based earthquake engineering methodology for reinforced concrete building structures*, Sapporo, Japan, 11–13 September, pp. 187–206.

Dávalos H and Miranda E (2019) Filtered incremental velocity: A novel approach in intensity measures for seismic collapse estimation. *Earthquake Engineering and Structural Dynamics* 48(12): 1384–1405.

Dávalos H and Miranda E (2020) Evaluation of FIV3 as an intensity measure for collapse estimation of moment-resisting frame buildings. *Journal of Structural Engineering* 146(10): 1–14.

Dávalos H and Miranda E (2021) A ground motion prediction model for average spectral acceleration. *Journal of Earthquake Engineering* 25(2): 319–342.

Dávalos H, Heresi P and Miranda E (2020) A ground motion prediction equation for filtered incremental velocity FIV3. *Soil Dynamics and Earthquake Engineering* 139: 106346.

Eads L and Miranda E (2013) *Seismic Collapse Risk Assessment of Buildings: Effects of Intensity Measure Selection and Computational Approach*. Report No. 184, Stanford University, Available at: https://stacks.stanford.edu/file/druid:wp898br0348/Eads_Dissertation-augmented.pdf

Eads L, Miranda E and Lignos DG (2015) Average spectral acceleration as an intensity measure for collapse risk assessment. *Earthquake Engineering & Structural Dynamics* 44(12): 2057–2073.

Gentile R and Galasso C (2021) Hysteretic energy-based state-dependent fragility for ground-motion sequences. *Earthquake Engineering & Structural Dynamics* 50(4): 1187–1203.

Hancock J and Bommer JJ (2006) A state-of-knowledge review of the influence of strong-motion duration on structural damage. *Earthquake Spectra* 22(3): 827–845.

HAZUS (2003) *Multi-hazard Loss Estimation Methodology—Earthquake Model*. Available at: https://www.fema.gov/sites/default/files/2020-09/fema_hazus_earthquake-model_technical-manual_2.1.pdf

Huang C and Galasso C (2019) Ground-motion intensity measure correlations observed in Italian strong-motion records. *Earthquake Engineering & Structural Dynamics* 48(15): 1634–1660.

Husid R (1969) Características de terremotos. Análisis general. *Revista IDIEM* 8(1): 21–42.

Iervolino I, Manfredi G and Cosenza E (2006) Ground motion duration effects on nonlinear seismic response. *Earthquake Engineering and Structural Dynamics* 35(1): 21–38.

Kaka SI and Atkinson GM (2004) Relationships between instrumental ground-motion parameters and modified Mercalli intensity in Eastern North America. *Bulletin of the Seismological Society of America* 94(5): 1728–1736.

Kazantzi AK and Vamvatsikos D (2015) Intensity measure selection for vulnerability studies of building classes. *Earthquake Engineering & Structural Dynamics* 44(15): 2677–2694.

Kingma DP and Ba J (2014) Adam: A method for stochastic optimization. In: *3rd international conference on learning representations ICLR*, pp. 1–15. Available at: http://arxiv.org/abs/1412.6980

Kohrangi M, Bazzurro P, Vamvatsikos D and Spillatura A (2017) Conditional spectrum-based ground motion record selection using average spectral acceleration. *Earthquake Engineering & Structural Dynamics* 46(10): 1667–1685.

Kohrangi M, Papadopoulos AN, Bazzurro P and Vamvatsikos D (2020) Correlation of spectral acceleration values of vertical and horizontal ground motion pairs. *Earthquake Spectra* 36(4): 2112–2128.

Kotha SR, Bindi D and Cotton F (2017) Site-corrected magnitude- and region-dependent correlations of horizontal peak spectral amplitudes. *Earthquake Spectra* 33(4): 1415–1432.

McCulloch WS and Pitts W (1943) A logical calculus of the ideas immanent in nervous activity. *The Bulletin of Mathematical Biophysics* 5(4): 115–133.

O'Reilly GJ (2021a) Limitations of Sa(T 1) as an intensity measure when assessing non-ductile infilled RC frame structures. *Bulletin of Earthquake Engineering* 19(6): 2389–2417.

O'Reilly GJ (2021b) Seismic intensity measures for risk assessment of bridges. *Bulletin of Earthquake Engineering* 19(9): 3671–3699.

Otárola K, Sousa L, Gentile R and Galasso C (2023) Impact of ground-motion duration on nonlinear structural performance: Part II: Site- and building-specific analysis. *Earthquake Spectra* 39(2): 860–888.

Oyarzo-Vera C and Chouw N (2008) Effect of earthquake duration and sequences of ground motions on structural responses. In: *Proceedings of the 10th international symposium on structural engineering for young experts*, ISSEYE, Changsha, China, 19–21 October, pp. 1881–1886.

Raghunandan M and Liel AB (2013) Effect of ground motion duration on earthquake-induced structural collapse. *Structural Safety* 41: 119–133.

Sarieddine M and Lin L (2013) Investigation correlations between strong-motion duration and structural damage. *Structures Congress* 2013: 2926–2936.

Spillatura A, Kohrangi M, Bazzurro P and Vamvatsikos D (2021) Conditional spectrum record selection faithful to causative earthquake parameter distributions. *Earthquake Engineering & Structural Dynamics* 50(10): 2653–2671.

Tarbali K and Bradley BA (2015) Ground motion selection for scenario ruptures using the generalised conditional intensity measure (GCIM) method. *Earthquake Engineering & Structural Dynamics* 44(10): 1601–1621.

Tarbali K, Bradley BA and Baker JW (2023) Effect of near-fault directivity pulses on ground-motion intensity measure correlations from the NGA-West2 data set. *Earthquake Spectra* 39(4): 2263–2280.

Trifunac MD and Brady AG (1975) A study on the duration of strong earthquake ground motion. *Bulletin of the Seismological Society of America* 65(3): 581–626.

Vamvatsikos D and Cornell CA (2005) Developing efficient scalar and vector intensity measures for IDA capacity estimation by incorporating elastic spectral shape information. *Earthquake Engineering and Structural Dynamics* 34(13): 1573–1600.

Wooddell KE and Abrahamson NA (2014) Classification of main shocks and aftershocks in the NGA-West2 database. *Earthquake Spectra* 30(3): 1257–1267.